INORGANIC CHEMISTRY
FRONTIERS

RESEARCH ARTICLE

View Article Online
View Journal | View Issue

Cite this: *Inorg. Chem. Front.*, 2023, **10**, 6357

Multimodal nanogels combining ZW800-1 as an optical absorber and gadolinium chelates for multispectral optoacoustic tomography (MSOT) and magnetic resonance imaging (MRI)†

Camille Gosée,[a,b] Juliette Moreau,[a] Cyril Cadiou,[a] Maité Callewaert,[a] Céline Henoumont,[b] Lionel Larbanoix,[c] Michael Molinari,[d] Sorina N. Voicu,[e] Christophe Portefaix,[f] Sophie Laurent *[b,c] and Françoise Chuburu *[a]

Received 22nd June 2023,
Accepted 11th September 2023

DOI: 10.1039/d3qi01167d

rsc.li/frontiers-inorganic

The challenge of imaging is to combine resolution and sensitivity in order to gain accuracy in diagnosis. No single modality can provide comprehensive information. Then, the solution is to design probes that are able to gather on a single platform the best features of the different imaging modalities. To achieve this objective, we have combined two types of probes, one associated with photoacoustic imaging (PAI) and the other with magnetic resonance imaging (MRI), within polysaccharide-based nanohydrogels. For that, chitosan (CS) which is a cationic polysaccharide was grafted with the photoacoustic probe ZW800-1. The synthesis of the corresponding CS-ZW800 and the purification conditions that allow to overcome ZW800 aggregation on the course of the protocol were carefully analyzed. Nanohydrogels that encapsulated gadolinium chelates as MRI probes were further obtained by ionic gelation between CS-ZW800 and the anionic hyaluronic acid (HA) in the presence of tripolyphosphate (TPP) as an ionogenic cross-linker. The bimodal nanohydrogels were then subjected to MSOT and MRI experiments. Upon excitation at 770 nm the nanoparticles were then able to produce a significant MSOT signal while in MRI at 3T, a significant positive contrast was obtained with low Gd doses.

1. Introduction

One of the challenges in *in vivo* imaging is to reveal the presence of pathological tissues as early as possible with a good resolution. Medical imaging techniques currently used in diagnosis either possess excellent resolution or are very sensitive but rarely cover both aspects.[1,2] Therefore, the solution is to combine imaging modalities with complementary characteristics that overcome the limitations of each imaging modality when used alone, to establish more precise diagnoses, guide the treatment of patients, and thus improve their prognosis.[3–5] In this goal, one solution is injecting a mixture of each probe and then acquiring the images inherent to each technique. The other is to combine the desired modalities in a single structure, which avoids artifacts due, for example, to different probes' bioavailability or biological half-lives.

In this latter approach, one of the solutions is to use the opportunities offered by nanotechnology to combine within the same nanoparticle, by encapsulation and/or grafting, the chemical entities associated with the chosen imaging modalities.[6,7] In these combinations, high-resolution images are obtained by magnetic resonance imaging (MRI). This non-invasive, non-radiative technique offers sub-millimeter spatial resolution and unlimited depth penetration, making it an essential technique for clinical diagnosis.[8] MRI takes advantage of the water abundance in the human body. Indeed, the physical principles of MRI rely on the magnetic water protons' relaxation times (the longitudinal T_1 and the transverse T_2 relaxation times), which depend on the magnetic field, the pulse sequence, on the heterogeneous distribution and environment of water within the defined volume under

[a]*University of Reims Champagne Ardenne, CNRS, ICMR UMR 7312, Reims, France. E-mail: francoise.chuburu@univ-reims.fr*
[b]*General, Organic and Biomedical Chemistry Unit, NMR and Molecular Imaging Laboratory, University of Mons, UMONS, B-7000 Mons, Belgium. E-mail: sophie.laurent@umons.ac.be*
[c]*Center for Microscopy and Molecular Imaging, University of Mons, Rue Adrienne Bolland 8, B-6041 Charleroi, Belgium*
[d]*CBMN CNRS UMR 5248, University of Bordeaux, INP Bordeaux, 33600 Pessac, France*
[e]*Faculty of Biology, Department of Biochemistry and Molecular Biology, University of Bucharest, Bucharest, Romania*
[f]*Radiology Department, CHU de Reims – Hôpital Maison Blanche, 45 Rue Cognacq-Jay, 51092 Reims Cedex, France*
† Electronic supplementary information (ESI) available. See DOI: https://doi.org/10.1039/d3qi01167d

investigation. All tissues have different T_1 (longitudinal) and T_2 (transverse) relaxation times, based on their water proton content and mobility within the tissues. Any change in the tissue will perturb the magnetic interactions between water protons leading to changes in its MRI contrast properties.[9] To increase the image contrast, paramagnetic contrast agents have been introduced. Most commercially available MRI contrast agents used for clinical examinations are gadolinium complexes in which the gadolinium ion is strongly sequestered by macrocyclic polyaminocarboxylate ligands to avoid its leakage *in vivo*.[10] The role of these gadolinium-based contrast agents (GBCAs) is to affect the longitudinal relaxation time T_1 of water protons in tissues and then to give rise to signal intensity increases (positive GBCAs). The efficiency with which GBCAs will catalyze the longitudinal relaxation of protons from tissue water molecules is quantified by the relaxivity r_1, which represents the enhancement of the longitudinal relaxation rate ($R_1 = {T_1}^{-1}$) of the water protons induced by one millimole per liter of GBCAs. In previous works, we have demonstrated that it was possible to strongly enhance the relaxivity of commercial GBCAs by encapsulating them within nanohydrogels, the consequence being a huge gain in MRI sensitivity.[11–13]

Even if hypersensitive MRI probes can be envisaged, the association of this technique with imaging modalities known for their sensitivity should be considered. Thus MRI combined with optical imaging (OI) or nuclear imaging such as positron emission tomography (PET) and single-photon emission computed tomography (SPECT) are tandem imaging modalities that already found clinical applications.[14,15] In the case of nuclear imaging, safety is an issue because of radiation concerns.[7] Consequently, for diagnostic purposes, non-ionizing radiation may be preferable to allow the collection of anatomical and/or functional information. In this respect, optical imaging exhibits very high sensitivity, but due to the high tissue photon absorbance of visible light (between 400 and 650 nm), the propagation of incident and emitted radiation by the fluorescent reporter agents is limited to few millimeters. This issue can be partially overcome by using near infrared (NIR) light (650–900 nm), which penetrates deeper into biological tissues (up to 2 cm). However, the spatial resolution of optical methods falls drastically with increasing tissue depth because of photons scattering, which limits the fluorescence visualization of fine biological details under the tissue surface. These pitfalls can be overcome with photoacoustic imaging (PAI). PAI is a non-invasive imaging modality that converts light application into ultrasonic signals (US) *via* the photoacoustic effect ('Light in – Sound out' concept)[16–19] Photoacoustic effect, described for the first time by A. G. Bell, has become very interesting, in particular for imaging because of the implementation of pulsed laser technology in the nanosecond range and sensitive acoustic detectors.[17] The photoacoustic effect starts then with the illumination of the tissue of interest with pulsed NIR light and is followed by homogeneous diffusion of photons within the tissue. The absorption of these photons leads to localized heating of the tissue causing thermal expansion and generation of pressure waves (ultrasound) that are finally detected by transducers. As ultrasounds are very weakly scattered and absorbed in biological tissues, PAI is therefore suitable for deep tissue applications (up to several centimeters) and fine localization in depth, and consequently it allows tomographic imaging at relatively high spatial resolution (150 μm).[17–19] As the laser pulses several times per second and each laser pulse generates an image, this technique is very fast and could be considered as real-time imaging in some setups.

Consequently, a multimodal probe combining MRI and PAI would have a significant interest to gather at the same time the spatial resolution of MRI, and the sensitivity and speed of PAI. In this work, we have designed a multimodal MRI/PAI probe by a combination of GBCA encapsulated within nanohydrogels functionalized with a NIR optical/photoacoustic probe, the ZW800-1 dye (Scheme 1). ZW800-1[20] is an exogenous luminophore that absorbs in the NIR range (λ_{abs}(maximum) = 772 nm) to allow maximum depth of investigation. Moreover, its spectral profile is sufficiently distinguishable from that of the endogenous chromophores (such as hemoglobin, melanin, lipids, myoglobin)[21] to be algorithmically separated using multispectral optoacoustic tomography (MSOT).[17,20–26] For that, nanohydrogels (NGs) were obtained by physical gelation between two polysaccharide biopolymers namely chitosan CS beforehand functionalized with ZW800-1 (CS-ZW800) and hyaluronic acid HA. This method relies upon the establishment of multivalent electrostatic interactions between CS-ZW800 (which is polycationic) and HA (which is polyanionic). The resulting supramolecular network can then be strengthened by cross-linking mediated by ionogenic cross-linkers such as sodium tripolyphosphate (TPP).[27] HGdDOTA, which is the active substance of DOTAREM® was incorporated within the nanogels, as the GBCA. After characterization of CS-ZW800 copolymer and HGdDOTA⊂CS-ZW800-TPP/HA nanogels, the photophysical and magnetic behaviors of these nanogels were investigated, before demonstrating the improvement of MRI and photoacoustic contrasts they provide.

2. Experimental section

2.1 General

Chitosan (CS, from shrimp shells, 51 kDa, viscosity = 33 mPa s in 1% acetic acid, 20 °C, deacetylation degree DD of 86%) was purchased from Sigma-Aldrich. Hyaluronic acid sodium salt (HA 1000 kDa extracted from *Streptococcus Equi* sp.), was purchased from Sigma-Aldrich.

Sodium tripolyphosphate (TPP) was purchased from Acros Organics. HGdDOTA (gadolinium(III)-1.4.7.10-tetraazacyclododecane-1.4.7.10-tetraacetate) was synthesized according to a published procedure.[11] Sterile water for injections (Laboratoire Aguettant, Lyon, France) was systematically used for polymer, nanoparticle preparations, and analyses.

Native and functionalized polymers (CS and CS-ZW800) were characterized by FTIR (Nicolet IS 5 spectrometer

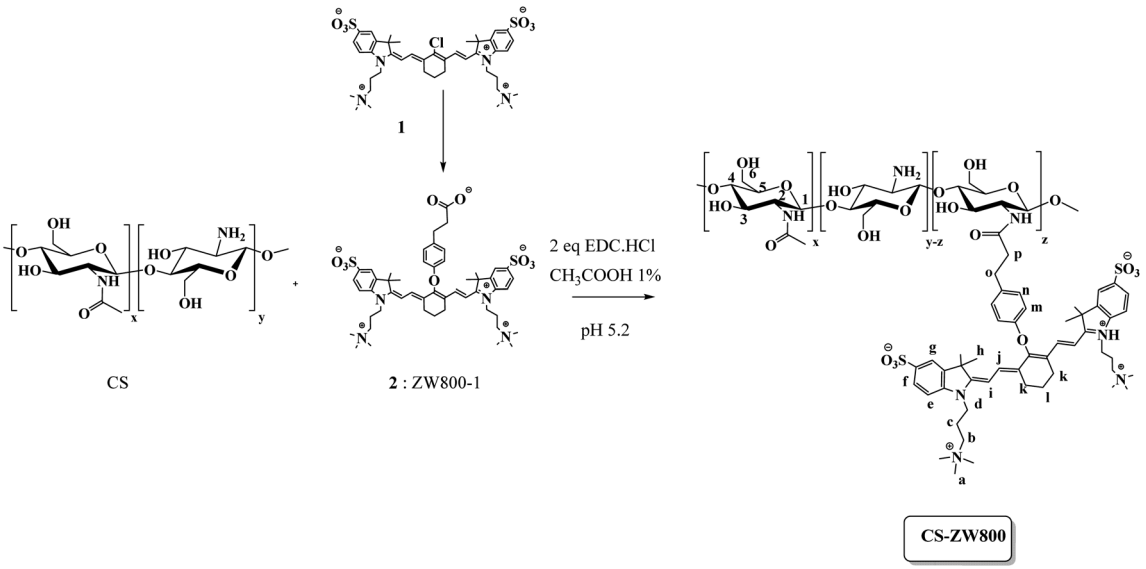

Scheme 1 Synthesis of CS-ZW800.

equipped with an ATR ID5 module), ^{1}H NMR (Bruker Avance III 500 MHz NMR spectrometer) at 318 K with D_2O/DCl (700/1, v/v) as a solvent, UV-visible and fluorescence spectroscopies (Varian Cary 5000 Shimadzu UV-2401PC and Varian Cary Eclipse, respectively). Centrifugation experiments were performed with an Alegra X-30 centrifuge (Beckman-Coulter).

2.2 Preparation of ZW800-1 dye from its chloro precursor

The zwitterionic chromophore ZW800-1 3-(4-(((*E*)-2-((*E*)-2-(3,3-dimethyl-5-sulfonato-1-(3-(trimethylammonio)propyl)-3*H*-indol-1-ium-2-yl)vinyl)-6-(2-((*E*)-3,3-dimethyl-5-sulfonato-1-(3-(trimethylammonio)propyl)indolin-2-ylidene)ethylidene)cyclohex-1-en-1-yl)oxy)phenyl) propanoate **2** was prepared according to the protocols previously described,[20,28] the last step of the synthesis involving a reaction of its chloro precursor **1** 2-((*E*)-2-((*E*)-2-chloro-3-(2-((*E*)-3,3-dimethyl-5-sulfonato-1-(3-(trimethylammonio) propyl)indolin-2-ylidene)ethylidene) cyclohex-1-en-1-yl)vinyl)-3,3-dimethyl-1-(3-(trimethylammonio)propyl)-3*H*-indol-1-ium-5-sulfonate with 3-(4-oxidophenyl)propanoate.

The purity of ZW800-1 **2** was controlled by elemental analysis, mass spectrometry, and ^{1}H NMR spectroscopy (Fig. S1†).

^{1}H NMR (500 MHz, D_2O/MeOD): δ 1.25 (s, 12H), 1.98 (m, 2H), 2.22 (m, 4H), 2.45 (m, 2H), 2.70 (m, 4H), 2.81 (m, 2H), 3.14 (s, 18H), 3.52 (m, 4H), 4.11 (m, 4H), 6.18 (d, J = 14 Hz, 2H), 6.98 (d, J = 8 Hz, 2H), 7.25 (m, 4H), 7.73 (s, 2H), 7.79 (d, 2H, J = 8 Hz), 7.96 (d, 2H, J = 14 Hz).

HRESI-MS (negative mode, H_2O): calculated for $C_{51}H_{65}N_4O_9S_2$ $[M - H]^-$ m/z 941.4193, found m/z 941.4200; m/z 882.3474 for $[C_{48}H_{56}N_3O_9S_2]^-$; m/z 621.2617 for $[C_{35}H_{45}N_2O_6S]^-$; m/z 325.1227 for $[C_{16}H_{25}N_2O_3S]^-$.

Elemental analysis: calculated for $C_{51}H_{66}N_4O_9S_2{\cdot}9H_2O$ (M = 1105.36 g mol^{-1}) C 55.42%, H 7.66%, N 5.07%, S 5.80% found C 55.45%, H 7.25%, N 4.96%, S 6.08%.

As the chitosan degree of substitution by ZW800-1 as well as the concentration of ZW800-1 present in the nanohydrogels will have to be determined, the molar extinction coefficient of ZW800-1 was re-determined by serial dilutions in acetate buffer (pH 4.7) (2×10^{-7} < [ZW800-1] < 10^{-6} mol L^{-1}, Fig. S2a†) and found to be equal to $\varepsilon_{767\ nm}$ = 108 652 L mol^{-1} cm^{-1}. $k_{fluorophore}$ being equal to the ratio between the emission intensity at 787 nm and the fluorophore concentration was also based on the basis of the previous solutions and found to be equal to $k_{ZW800,\ 787\ nm} = 3.58 \times 10^8$ mol^{-1} L (Fig. S2b†).

2.3 Preparation and characterization of CS-ZW800 polymer

CS (100 mg, 0.50 mmol of NH_2 function) was dissolved in 5 mL of acetic acid 1% (v/v). After complete CS dissolution, the pH was adjusted to 5 by the addition of 1 M NaOH and the resulting solution was allowed to stir for 1 h. ZW800-1 and 2 equivalents of EDC, HCl were solubilized in 2.5 mL of ultrapure water (ZW800-1/NH_2 CS molar ratio expressed as % mol $(COOH/NH_2)_{initial}$ of 5 and 10%, corresponding to 28 and 55.5 mg of ZW800-1 and 10 and 20 mg of EDC, HCl, respectively). This solution was stirred for 1 h to activate the ZW800-1 carboxylic function, and then, was added dropwise to the CS solution. The final mixture was stirred, protected from light, at room temperature for 36 h. At the end of the reaction, CS-ZW800 was purified by cross flow-filtration[29] (MicroKros hollow fiber modules, pores of 0.1 μm) before freeze drying, to finally recover CS-ZW800 as a green foam. For alternative purification procedures, please refer to the text and to the ESI† for UV-visible spectroscopy monitoring of these steps (Fig. S5†).

FT-IR (ATR, cm^{-1}): 3356–3285 (ν_{OH} and ν_{NH}), 2923–2876 (ν_{CH}), 1643 (amide I), 1559 (amide II), 1403–1376 (δ_{CH}), 1163 (ν_{COC}) and 1059–1015 (ν_{CO}) cm^{-1}.

^{1}H NMR (500 MHz, 318 K, D_2O/DCl: 700 μL/1 μL – Fig. S7†), δ (ppm): 1.21 (s, CH_3 – ZW800-1: H_h), 2.0–2.1 (s, CH_3COO^-

and CH_3 – CS acetyl units), 2.90 (s, CH_3 – ZW800-1, H_a), 3.18 (s, 1H – CS, H_2), 3.5–4.2 (m, 5H – CS, H_{3-6}), 4.87 (s, 1H – CS, H_1), 6.13 (d, J = 14 Hz – ZW800-1, H_i), 7.03 (d, J = 8 Hz – ZW800-1, H_e), 7.15–7.30 (m – ZW800-1, H_m, H_n), 7.72 (s – ZW800-1, H_g), 7.80 (d, J = 8 Hz – ZW800-1, H_f), 7.91 (d, J = 14 Hz – ZW800-1, H_j).

The association rate of ZW800-1 to CS chains in CS-ZW800 samples was determined, after purification by UV-visible or fluorescence spectroscopies. The association rate is the total amount of dye which corresponded to the ratio between the sum of the grafted dye (ZW800-1_G) and the ungrafted one (ZW800-1_{UG}), and the amount of CS. For this purpose, the absorbance at 767 nm or the emission intensity at 787 nm of 0.13–0.05 mg mL^{-1} solutions of CS-ZW800 (in a pH 4.7 acetate buffer) were measured (Varian Cary 5000 and Varian Cary Eclipse spectrometer, with λ_{exc} = 760 and $\Delta\lambda_{exc} = \Delta\lambda_{em}$ = 5 nm for absorption and emission measurements, respectively). This ratio (ZW800-1_T/CS) was calculated according to eqn (1).

$$\%\left(\frac{\text{ZW800-1}_T}{\text{CS}}\right)_{mol} = \frac{A_{ZW800}/(\varepsilon_{ZW800\text{-}1\times l})(\text{or } I_{ZW800\text{-}1}/k_{ZW800\text{-}1})}{m_{CS\text{-fluorophore}}/\left(M_{CS_{rep\ unit}} \times V\right)} \times 100 \quad (1)$$

with $A_{ZW800\text{-}1}$ and $I_{ZW800\text{-}1}$ being the absorbance and emission intensity measured at 767 and 787 nm, respectively, $\varepsilon_{ZW800\text{-}1}$ and $k_{ZW800\text{-}1}$ being the molar extinction coefficient (at 767 nm) and the proportionality factor between the emission intensity (at 787 nm) and ZW800-1 concentration, respectively.

The fluorescence quantum yield of CS-ZW800, determined in acetate buffer pH 4.7 with an integration sphere was Φ = 9%.

The chitosan degree of substitution (DS_{CS}) was determined by DOSY experiments, according to a procedure described elsewhere.[13] In this procedure, the diffusion coefficients of chitosan and ZW800 were fixed at 1×10^{-11} m^2 s^{-1} and 4.65×10^{-10} m^2 s^{-1} respectively.

2.4 Preparation and characterization of CS-ZW800-TPP/HA and GdDOTA⊂CS-ZW800-TPP/HA nanohydrogels

Nanohydrogels have been prepared by ionic gelation following a method previously developed in our group.[13] Briefly, the polyanionic aqueous phase (4.5 mL) containing both HA (0.8 mg mL^{-1}) and TPP (1.2 mg mL^{-1}) was added dropwise to the CS-ZW800 solution (22.5 mg dissolved in 9 mL of 10% v/v acetic acid solution, ZW800-1/NH_2 CS = 1.68 and 0.78%) under sonication (750 W, amplitude 32%). At the end of the addition, magnetic stirring was maintained for 10 min. Purification and pH correction of the nanosuspensions were achieved using cross flow-filtration[29] (Spectrum®MicroKros hollow fiber modules, cut-off of 0.1 μm with 4 cycles of dilution-concentration by a factor of 2). Gadolinium loaded nanogels (GdDOTA⊂CS-ZW800-TPP/HA NGs) were prepared in the same way, by incorporating HGdDOTA (17 mg) as the MRI contrast agent in the anionic phase.

The nanogels averaged hydrodynamic diameters (Z-ave) were determined by Dynamic Light Scattering (DLS) with a Zetasizer Nano ZS (Malvern Zetasizer Nano-ZS, Malvern Instruments, Worcestershire, UK). Each sample was analyzed in triplicate at 20 °C at a scattering angle of 173°, after a 1/20 dilution in water. Water was used as a reference dispersing medium. ζ-(Zeta) potential data were collected through Electrophoretic Light Scattering (ELS) at 20°C, 150 V, in triplicate for each sample, after a 1/20 dilution in water. The instrument was calibrated with a Malvern – 68 mV standard before each analysis cycle.

These analyses were completed by Atomic Force Microscopy (AFM). Each sample was analyzed in triplicate at a controlled temperature of 20°C. To be observed, 20 μL of the nanosuspension was deposited on a freshly cleaved mica and incubated for 15 minutes. The samples were rinsed five times with 100 μl of mQ water. All the experiments were performed in water (150 μL) to avoid nanogel drying. AFM imaging was then performed on a Bruker Fastscan setup (BrükerNano, Santa Barbara, USA) in Peak Force Tapping mode with MSNL-E probe with a nominal spring constant of 0.07 N m^{-1}, a nominal frequency of 22 kHz and a nominal tip radius of 2 nm. In order to remain in good tracking conditions but to avoid particle damaging, a PeakForce setpoint of 100 pN was used. For image processing, the Nanoscope Analysis 1.8 software (Bruker, Billerica, USA) was used.

Gadolinium nanoparticle loadings were determined on purified nanosuspensions by Inductively Coupled Plasma – Optical Emission Spectroscopy (ICP-OES). The non-encapsulated complexes were separated from the NGs by high-speed centrifugation for 1 h 15 min at 4°C and 23 200g (Beckman Avanti™ J-E Centrifuge, France). The resulting NG pellet was then incubated overnight in a 1 : 3 (v/v) mixture of HCl (37%) and HNO_3 (69%) to release Gd from the polymer matrix and the complexes. After the NG destruction, volumetric dilutions were carried out to achieve an appropriate Gd concentration within the detection range of the method. Similar procedure was implemented to determine Gd content in supernatants. Samples were analyzed using ICAP 6000 series ICP-OES spectrometer. Counts of Gd were correlated to a Gd calibration curve generated by mixing $Gd(NO_3)_3$ standard with unloaded NGs incubated under the same acidic conditions.

The fluorescence quantum yields of CS-ZW800-TPP/HA and GdDOTA⊂CS-ZW800-TPP/HA nanohydrogels determined in acetate buffer pH 4.7 with an integration sphere were identical and equal to Φ = 2%.

In vitro cytotoxicity of GdDOTA⊂CS-ZW800-TPP/HA nanogels was tested by means of a MTT assay.[30] RAW 267.4 cell line (adherent cells) purchased from American Type Culture Collection (ATCC catalog no., TIB-7), were cultured in Dulbecco Modified Eagle Medium (DMEM, Gibco/Invitrogen, Carlsbad, CA, USA) pH 7.4 with 4 mM L-glutamine adjusted to contain 4.5 g L^{-1} glucose and, 1.5 g L^{-1} sodium bicarbonate. The growth medium was supplemented with 10% fetal bovine serum, 1% antibiotics (penicillin, streptomycin, amphotericin) and cells were maintained at 37°C in a humidified atmosphere

(95%) with 5% CO_2. The cells seeded in 24-well plates at a density of 10^5 cells per mL were incubated for 24 and 48 hours at different concentrations of CS-ZW800-TPP/HA and GdDOTA⊂ CS-ZW800-TPP/HA nanogels (*i.e.* 2.5, 5, 10, 25 and 50 μg mL^{-1}). Cell viability was measured by the MTT, 3-(4,5-dimethylthazol-2-yl)-2,5-diphenyl tetrazolium bromide, assay. After the exposure time, the culture medium was removed and in each well were added 500 μL MTT (1 mg mL^{-1}) for 2 hours. After that, the MTT solution was removed and the formazan crystals were solubilized in 100% isopropanol. The optical density was measured at 595 nm using Flex Station 3 Multi-Mode Microplate Reader. The cell viability was expressed in percentage considering 100% viability for control cells.

2.5 Nuclear magnetic relaxation dispersion (NMRD) profiles and 3T MR imaging (MRI)

2.5.1 NMRD profiles. ^{1}H NMRD profiles were measured on a Stelar Spinmaster FFC fast field cycling NMR relaxometer (Stelar, Mede, Pavia, Italy) over a range of magnetic fields extending from 0.48 mT to 0.7 T and corresponding to ^{1}H Larmor frequencies from 0.02 to 30 MHz using 0.5 mL samples in 7.5 mm o.d. tubes. The temperature was kept constant at 37°C. An additional relaxation rate at 60 MHz was obtained with a Bruker Minispec mq60 spectrometer (Bruker, Karlsruhe, Germany). The diamagnetic contribution of unloaded particles was measured and subtracted from the observed relaxation rates of the Gd-loaded nanoparticles.

2.5.2 MR imaging. MR imaging of NP suspensions were performed using a 3.0 T MRI device (Skyra, Siemens Healthcare, Erlangen, Germany) with a 15 channel transmit/receive knee coil. T_1-Weighted images were obtained with an 3D fast spin-echo T_1 sequence (TR = 700 ms, TE = 12 ms, FOV = 201 × 201 mm, matrix = 256 × 256, voxel size = 0.78 × 0.78 × 2 mm). T_2-Weighted images were obtained with an 3D fast spin-echo T_2 sequence (TR = 1000 ms, TE = 103 ms, FOV = 199 × 199 mm, matrix = 384 × 384, voxel size = 0.52 × 0.52 × 0.55 mm). The gadolinium concentrations were tested in the 25–200 μM range.

2.6 Multispectral optoacoustic tomography (MSOT)

MSOT data were acquired using a InVision 256-TF scanner (iThera Medical, Germany) equipped with tunable Nd:YAG laser that provides 9 ns excitation pulses with a peak energy of 90 mJ at 720 nm at a repetition rate of 10 Hz. Laser generates light of wavelengths ranging from 660 to 1300 nm that is carried by 10 optical fibers to provide 360° uniform illumination of the phantom. Ultrasound waves are detected by 256 toroidally focused ultrasound transducers with a center frequency of 5 MHz that are organized in a concave array of 270-degree angular coverage to provide cross-sectional images. *In vitro* sample measurements were performed using the durable phantom (iThera Medical) that is scattering. The right well was filled with 200 μL of sample suspension, while the left well was filled with water as reference. PA spectra were collected by scanning from 660 nm to 850 nm wavelength range with 5 nm increments at 25 °C, with 3 averages. Data were analyzed using viewMSOT 4.0 software (iThera Medical); a circle region of interest (ROI) was draw in the center of wells to quantify the PAI signal intensity (arbitrary units, a.u.) and determined the PAI spectra.

3. Results and discussion

3.1 CS-ZW800 polymer preparation

CS-ZW800 polymer was synthesized by a conventional peptidic coupling between the amino group of the CS glucosamine residue and the carboxylic function of the dye ZW800-1, in the presence of EDC·HCl as the coupling agent (Scheme 1). To check the influence of the initial proportion between ZW800-1 and amino function of CS (expressed as ZW800-1/NH_2 CS molar ratio), two ratios of 5 and 10% were respectively tested. UV-visible spectra of the crude product exhibit beside the expected signals of ZW800-1 (700 nm (shoulder) and 770 nm), two additional absorptions with maxima at 450 and 610 nm respectively (Fig. S3†). The ether linkage on the meso carbon of the heptamethine core of ZW800-1 is known to be fragile.[31] The breaking of this bond induces a modification of the absorption spectrum with the appearance of a signal centered at 450 nm.[31] Thus, the first signal observed at 450 nm for the crude CS-ZW800 could be the fingerprint of ether bond breaking during the grafting reaction. It should be noted that the UV-visible spectrum of the chlorinated precursor of ZW800-1 (compound **1**, Scheme 1) exhibits, in addition to the characteristic signals of the heptamethine core, absorption at 430 nm (Fig. S4†) which reinforces the hypothesis that the ether bond of ZW800-1 was broken during the grafting reaction. The second signal at 610 nm, which is blue-shifted compared to the ZW800-1 signals, should be related to the formation of H-aggregates, as previously described for ZW800-1 analogs.[31] Consequently, it was necessary to implement a purification procedure to avoid the presence of any by-product or dimer from ZW800-1, which could be deleterious either to the formation of nanoparticles or to the interpretation of the MSOT signal.

3.2 Purification, IR, and ^{1}H NMR characterizations of CS-ZW800 polymer

Several purification techniques were therefore implemented. First, the polymer was purified by NaOH precipitation, which resulted in the reinforcement of the formation of H-aggregates (predominant signal in UV-visible spectroscopy around 600 nm, Fig. S5a†). Dialysis against water was not able to remove these aggregates (Fig. S5b†). In contrast, steric exclusion chromatography or tangential filtration have proven to be the methods of choice for obtaining CS-ZW800 polymer in adequate quantities without the presence of H-aggregates (Fig. S5c and 5d†). After workup and freeze-drying, CS-ZW800 samples were characterized by FT-IR (Fig. S6†). The main absorption bands specific of CS-ZW800 appeared around 3300 (ν_{OH} and ν_{NH}), 2900 (ν_{CH}), 1643 (amide I), 1559 (amide II), and 1163 cm^{-1} (C–O–C pyranose ring). ^{1}H NMR spectroscopy of

CS-ZW800 (Fig. S7†), in addition to chemical shifts corresponding to CS backbone or acetyl protons (pyranose ring proton H_2 of at δ = 3.18 ppm and H_3 to H_6 at δ = 3.5–4.2 ppm, anomeric proton H_1 at δ = 4.87 ppm and acetyl protons at δ = 2.0–2.1 ppm), confirmed the presence of ZW800-1 moiety in CS-ZW800 samples (H_a at δ = 2.9 ppm, H_h at δ = 1.21 ppm, ethylenic protons H_i and H_j at δ = 6.13 ppm and δ = 7.91 ppm respectively and H_{ar} at δ = 7.0–7.8 ppm). The total amount of ZW800-1 associated to CS chains was estimated by absorption and emission spectroscopies (Table S8†). With the uncertainties inherent to each method, the % of association are concordant and on average 2.75% for a $(ZW800\text{-}1/CS)_{ini}$ ratio of 10% and 1.20% for a $(ZW800\text{-}1/CS)_{ini}$ ratio of 5%. In addition, DOSY experiments run on CS-ZW800 polymer for which the % of ZW800-1 associated to CS chains was estimated in average to 2.75%, indicate that at least 61% of the dye is grafted to the polymer, leading to a CS degree of substitution (DS_{CS}) of 1.68% (Table S9†). For the second sample for which the % of ZW800-1 associated to CS chains was estimated in average to 1.20%, DOSY measurements led to a DS_{CS} of 0.78% (Table S9†). These ratios are closed to the ones obtained when CS was functionalized CS with fluorophores such as rhodamine or fluorescein.[13] They indicate that few NH_2 functions were functionalized by ZW800-1 leading enough protonable functions to obtain nanoparticles by ionic gelation.

3.3 Nanogels syntheses with functionalized CS-ZW800 polymer and characterizations and proof of concept as MSOT/MRI probes

3.3.1 Nanogels syntheses and morphological characterizations. Functionalized CS in association with HA and TPP was used to synthesize by physical gelation in a one-step procedure, CS-ZW800-TPP/HA nanogels. This method relies upon the establishment of multivalent electrostatic interactions between HA derivatives (polyanionic) and CS (polycationic). The resulting supramolecular network can be reinforced by cross-linking mediated by small anionic cross-linkers such as sodium tripolyphosphate (TPP).[27,32] Functionalized CS with various DS_{CS} (ZW800-1/CS = 1.68% and 0.78%) were then evaluated for their ability to produce functionalized CS-ZW800-TPP/HA NPs by ionic gelation. Functionalized CS-ZW800-TPP/HA nanogels formation was evidenced by DLS. The average hydrodynamic diameters of NPs were determined by dynamic light scattering (DLS, Table 1) recording hydrodynamic diameters and polydispersity index (PDI) of the nanosuspensions. Nanoparticle zeta potential (ζ) which was indicative of their outermost surface charge was determined by ELS. Before purification, the nanoparticles in the suspension have an average hydrodynamic diameter of 300 nm and a surface charge of 46 mV (Table 1). The polydispersity index of the sample is 0.26 which reveals a relatively homogeneous nanoparticle population. A first purification test by dialysis resulted in flocculation of the nanosuspension. Consequently, a tangential filtration method was implemented to purify the nanosuspension. This time, no flocculation was observed and the nanoparticles analyzed after filtration had a mean diameter of 312 nm, a surface charge of 46 mV and the polydispersity index of the nanosuspension is 0.28.

Similar characteristics are obtained for GdDOTA⊂CS-ZW800-TPP/HA nanogels incorporating the MRI contrast agent HGdDOTA (Table 1). This macrocyclic gadolinium chelate, which is the active substance of DOTAREM® is characterized by high thermodynamic and kinetic stability. This choice is driven by the fact that HGdDOTA is recognized as low-risk towards nephrogenic systemic fibrosis (NSF) in renal impaired patients[33] and its macrocyclic structure helps to prevent gadolinium leakage and subsequent deposition in the brain.[34] These nanogels have a slightly larger diameter which can be correlated with the incorporation of HGdDOTA within the nanoparticles. For some samples, AFM images in liquid mode corroborated the formation of globular object by evidencing nano-assemblies of lower size (few tens of nanometers) and the presence of some aggregates (Fig. S10†). Such differences between DLS and AFM measurements have already been

Table 1 Intensity weighted (*Z*-average) diameters, polydispersity indexes (PdI), and zeta potential (ζ) of a – CS-ZW800-TPP/HA and b – GdDOTA⊂CS-ZW800-TPP/HA nanogels according to CS degree of substitution (DS_{CS})

a – CS-ZW800-TPP/HA nanogels

	Z-Ave ± sd (nm)		PdI ± sd		ζ ± sd (mV)	
DS_{CS} [%]	i	ii	i	ii	i	ii
1.68	300 ± 6	312 ± 15	0.26 ± 0.03	0.28 ± 0.02	+46 ± 1	+46 ± 2
0.78	334 ± 11	373 ± 8	0.30 ± 0.01	0.30 ± 0.01	+53 ± 1	+53 ± 1

b – GdDOTA⊂CS-ZW800-TPP/HA nanogels

	Z-Ave ± sd (nm)		PdI ± sd		ζ ± sd (mV)	
DS_{CS} [%]	i	ii	i	ii	i	ii
1.68	325 ± 10	366 ± 27	0.30 ± 0.03	0.31 ± 0.02	+47 ± 1	+46 ± 2
0.78	359 ± 3	393 ± 3	0.34 ± 0.02	0.30 ± 0.02	+51 ± 1	+52 ± 1

i – before purification, ii – after purification.

observed for nanogels[35] and are attributed to the fact that in DLS, because of the presence of aggregates, the response could be biased by the use of mathematical models of signal processing.

3.3.2 Determination of ZW800 and Gd concentrations within the nanogels. The presence of ZW800-1 in the nanogels CS-ZW800-TPP/HA and GdDOTA⊂CS-ZW800-TPP/HA was confirmed by UV-visible titration (Table 2a). A decrease in ZW800-1 concentration between unpurified and purified nanogels is observed which can be attributed to the elimination of the free functionalized polymer. Indeed, the yield of nanoparticle production is estimated around 60%.

The concentration of gadolinium contrast agent embedded within GdDOTA⊂CS-ZW800-TPP/HA NGs was then evaluated by Gd titration by ICP-OES (Table 2b). Before purification, 7% (in concentration) of the gadolinium chelates were loaded within the nanogels. After purification, the concentration of chelates is almost maintained inside the nanogels while the concentration in the supernatant is clearly decreased. These results therefore show that purification by tangential filtration allows the removal of part of the complex not directly encapsulated in the gel and is gentle enough not to wring out the nanoparticles and empty them of their content.

3.3.3 MTT assay. Before evaluating CS-ZW800-TPP/HA and GdDOTA⊂CS-ZW800-TPP/HA NGs to promote a photoacoustic and a magnetic signal in MSOT and MRI respectively, the biocompatibility of these nanogels was controlled by means of MTT assay (Fig. S11†). For that, a murine macrophage cell line (RAW 264.7) was chosen, since macrophages are among the major cells mediating the inflammatory response to foreign substances, especially nanoparticles.[36] The incubation of RAW264.7 cells with both types of nanogels did not affect the cell survival during the tested period. Furthermore, this absence of toxicity is similar to the one observed for the non-fluorescent and fluorescent analogues[37,38] which highlighted that ZW800-1 grafting, while providing additional imaging functionality, did not affect the harmlessness of nanogels to cells.

3.4 *In vitro* imaging experiments with CS-ZW800-TPP/HA and GdDOTA⊂CS-ZW800-TPP/HA nanogels

3.4.1 Photoacoustic properties. The photoacoustic (PA) properties of CS-ZW800-TPP/HA and GdDOTA⊂CS-ZW800-TPP/HA were analyzed by using a inVision 256-TF imaging station (iThera Medical). The PA profiles of the nanogels as obtained by scanning over a wavelength range of 680–850 nm show that ZW800 nanogels display an intense peak at 770 nm (Fig. 1). Moreover, PA profiles of CS-ZW800-TPP/HA and GdDOTA⊂CS-ZW800-TPP/HA nanosuspensions have a similar intensity for a same concentration in dye (5 μM). It is also remarkable that for a similar concentration of ZW800-1 (5 μM), a PA signal of higher intensity is observed for nanoparticles by comparison to the pure dye. When ZW800 is incorporated within nanohydrogels, the enhancement of its PA signal is probably associated with ZW800 fluorescence quenching under the same conditions. Indeed, a quenching of the fluorescence emission for CS-ZW800-TPP/HA and GdDOTA⊂CS-ZW800-TPP/HA nanosuspensions was observed when compared to that of equivalent concentrations of the free dye resulting in a *ca.* 4.5 fold decrease of quantum yield. We can therefore assume that when the probe is embedded in the hydrogel, the radiative de-excitation mechanisms of the ZW800 probe, which compete with the photoacoustic phenomenon, are thus limited in favor of the light-to-soundwave conversion mechanism.

In a second step, the *in vitro* phantoms of ZW800-1 loaded nanoparticles were spatially scanned at 770 nm (Fig. 2), which corresponds to the maximum intensity of the PA signal in the spectral scans.

Table 2 a – ZW800-1 concentrations and b – Gd loadings of CS-ZW800-TPP/HA and GdDOTA⊂CS-ZW800-TPP/HA nanogels according to CS degree of substitution (DS_{CS})

a – [ZW800-1] (mol L^{-1})

	CS-ZW800-TPP/HA		GdDOTA⊂CS-ZW800-TPP/HA	
DS_{CS} (%)	i	ii	i	ii
1.68	2.04×10^{-4}	1.18×10^{-4}	2.07×10^{-4}	1.43×10^{-4}
0.78	8.40×10^{-5}	6.62×10^{-5}	8.02×10^{-5}	6.63×10^{-5}

b – [Gd] (mol L^{-1})

	GdDOTA⊂CS-ZW800-TPP/HA					
	Pellet		Supernatant		Total	
DS_{CS} (%)	i	ii	i	ii	i	ii
1.68	1.6×10^{-4}	1.2×10^{-4}	2×10^{-3}	5.7×10^{-4}	2.1×10^{-3}	6.9×10^{-4}
0.78	1.4×10^{-4}	1.3×10^{-4}	2×10^{-3}	4.7×10^{-4}	2.1×10^{-3}	5.9×10^{-4}

i – before purification, ii – after purification.

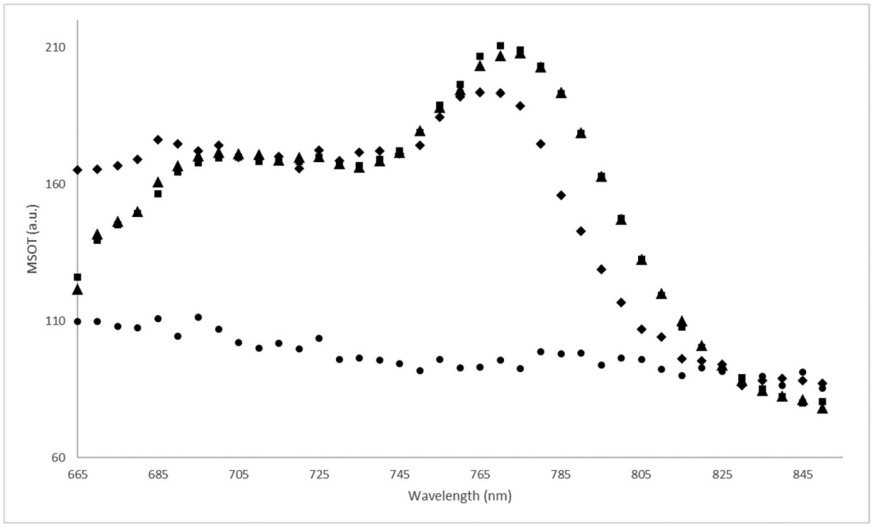

Fig. 1 PA spectral scans of CS-ZW800-TPP/HA (■), GdDOTA⊂CS-ZW800-TPP/HA (▲) nanogels, and ZW800 (◆) (● NaCl control).

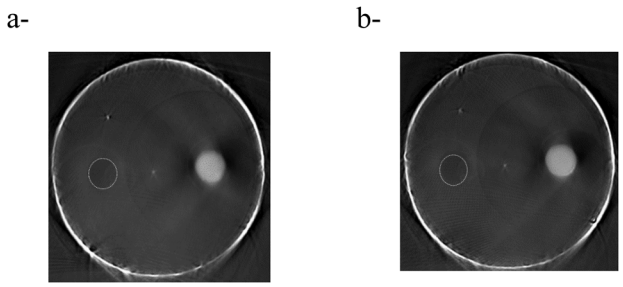

Fig. 2 MSOT phantoms of a – CS-ZW800-TPP/HA and b – GdDOTA⊂CS-ZW800-TPP/HA nanogels ($[ZW800\text{-}1]_{nanogels}$ = 5 μM) in the right well. Water reference in the left well, highlighted in dotted lines.

As the spectral scans suggested, CS-ZW800-TPP/HA and GdDOTA⊂CS-ZW800-TPP/HA nanogels provide contrasts of similar intensities which tends to indicate that the presence of Gd chelates does not modify the echogenic properties of the nanogels. This is a good starting point for the use of these probes in bimodal MSOT/MRI imaging.

3.4.2 Magnetic properties. The ability of these nanogels to increase contrast in MRI remains to be assessed. To evaluate the ability of nanogels to boost the relaxivity of HGdDOTA, the longitudinal relaxation rate of GdDOTA⊂CS-ZW800-TPP/HA nanogels was recorded at 37 °C, as a function of proton resonance frequency (Fig. 3a).

By comparison to HGdDOTA alone, the GdDOTA⊂CS-ZW800-TPP/HA NMRD profile shows a maximum in relaxivity (30 mM^{-1} s^{-1}). The signal shape is typical of those obtained when gadolinium chelates are embedded in polysaccharide-based hydrogels.[11–13,35,38–41] Moreover, one should notice that the profile shape is maintained over a period of 28 days (Fig. 3a), which demonstrated the stability of GdDOTA⊂CS-ZW800-TPP/HA nanogels as well as their ability to contain their Gd loading over the time. This great signal enhancement must be correlated with an important restriction of the chelates rotational motions inside the gel matrix.[9] Furthermore, the hydrophilic nature of CS and HA[42] that constituted the nanogel polymer matrix allowed a high water content, leading to a strong outer-sphere and/or second-sphere contribution to the relaxivity. We and others have also demonstrated that the presence of HA in the hydrogel matrix can significantly amplify the magnetic properties of the encapsulated GdDOTA.[12,41] HA is known as a highly hydrated polymer and its hydration is organized in several layers according to the nature of the interaction of HA chains with water (bound water layer, unbound water layer and free water layer). Thermodynamic measurement[40,41] have demonstrated that this organization can be perturbed by the presence of gadolinium chelates that interpose themselves between the water molecules and HA chains. This alteration mainly affects the bound water layer, creating water compartments that include gadolinium chelates, these chelates being subjected to osmotic pressure of swollen gels.[41] Therefore, this spontaneous generation of water-gadolinium clusters in the hydrogel matrix results in high MRI relaxation properties of the corresponding metallogels. Finally, this signal amplification is found on T_1-weighted MR images (Fig. 3b). For the same concentration range, a more intense contrast is observed when HGdDOTA is present in the nanogels than when it is free in solution. Furthermore, for the T_2-weighted images, under the same conditions, image darkening was observed (Fig. 3c). This important T_2 effect at high magnetic field results from the slow rotation of the encapsulated complexes and/or magnetic susceptibility effects.[43] Finally, by comparison with systems based on molecular architectures combining similar probes,[44] the performances of GdDOTA⊂CS-ZW800-TPP/HA nanogels in MSOT and MRI are better, which confirms the interest in

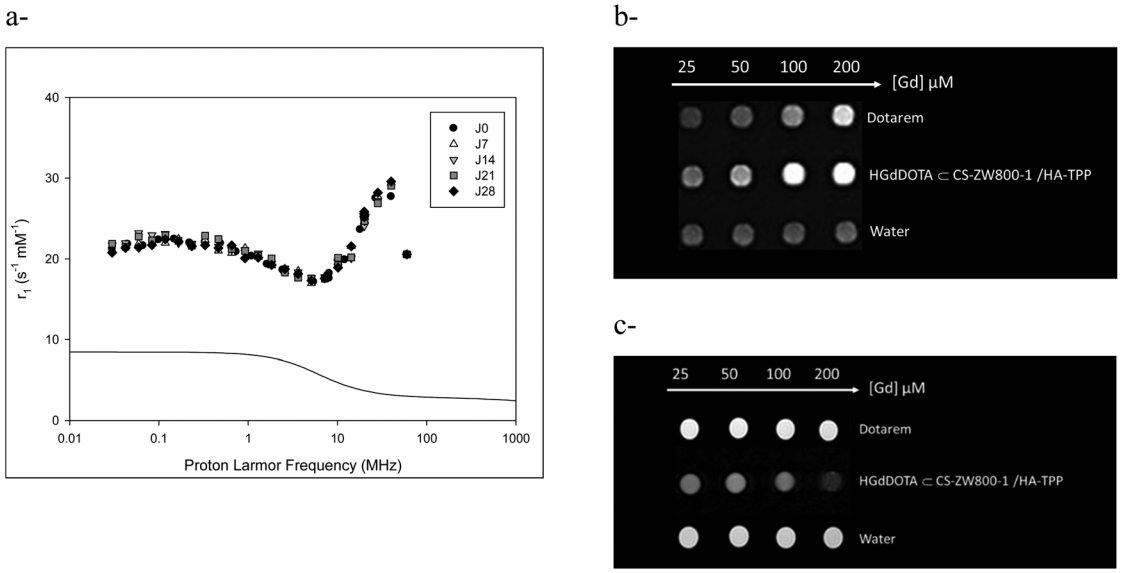

Fig. 3 a – NMRD relaxivity profile of GdDOTA⊂CS-ZW800-TPP/HA nanogels at 37 °C (solid line = HGdDOTA at 37 °C), b – T_1 and c – T_2 weighted images of GdDOTA⊂CS-ZW800-TPP/HA nanogels (3T).

using nanogel-type structures to develop high-performance imaging probes.

4. Conclusion

In this work the preparation of bimodal nanohydrogels, combining MRI and PA properties was described and their efficiency in both imaging modalities was demonstrated. For that, chitosan CS grafted with a NIR-absorber (ZW800-1), and carefully purified by cross-flow filtration in order to avoid ZW800 stacking leading to the formation of high energy absorbing H-aggregates, was associated to hyaluronic acid HA in a ionic gelation process. GdDOTA was incorporated within the corresponding nanogels during the process. The corresponding CS-ZW800-TPP/HA and GdDOTA⊂CS-ZW800-TPP/HA were fully characterized *in vitro* and their PA and MRI signals respectively recorded. Whatever the nanohydrogels, ZW800 PA signal was greater when it was grafted to the nanoparticle by comparison to a ZW800 solution of the same concentration. Similarly, GdDOTA MRI signal (evaluated through NMRD profiles and 3T MR imaging) was greatly amplified when the contrast agent was encapsulated within the nanohydrogels. This effect was attributed to the spontaneous generation of water-gadolinium clusters in hydrogel matrix (hydrodenticity concept). Finally, MTT tests carried out on the different nanohydrogels showed that they did not present any proven toxicity. Therefore we can conclude that the easy-to-synthesize biocompatible GdDOTA⊂CS-ZW800-TPP/HA nanohydrogels could constitute interesting contrast agents with greatly enhanced performances in terms of sensitivity and resolution for imaging. Finally, as the polymers used to produce nanogels can be easily functionalized, grafting systems to ensure stealth of nanoparticles could be envisaged. If we are to take into account the *in vivo* fate of nanogels before they do their work, we need to be concerned first and foremost with their lifetime in the bloodstream (at least if we are considering intravenous administration). The first step is their opsonization and their recognition by the RES system. In order to prevent the formation of a protein corona, our first intention is to pegylate the nanogels, and work is underway in this area. We are also aware that this solution needs to be improved because it is well known now, that when they are repeatedly administered, they can lose their long-circulation properties because of an accelerated blood clearance phenomenon. This is why we are also considering alternatives to PEG by replacing it with poly (phosphoester)s or zwitterionic polymers. Work in this area is currently underway.

Author contributions

Camille Gosée carried out all the syntheses and characterizations of the polymers and nanoparticles described in the manuscript. Juliette Moreau designed the functionalized polymer synthesis and purification protocols, as well as the protocols for dye quantification on grafted polymer. Cyril Cadiou optimized the dye synthesis protocol and worked on writing the manuscript. Maité Callewaert designed the nanohydrogels synthesis and purification protocols and supervised the preparation of the NMRD MSOT and MRI experiments. Céline Hénoumont carried out and analyzed the NMRD profiles. Lionel Larbanoix carried out and analyzed the MSOT experiments. Michael Molinari designed the AFM analysis protocol and recorded the corresponding images. Sorina Voicu designed and carried out the experiments demonstrating the biocompatibility of nanohydrogels. Christophe Portefaix designed the MRI analysis protocol and recorded the corres-

ponding images. Sophie Laurent was instrumental in finding the necessary funding for the study, and supervised the entire process. Françoise Chuburu also helped find the necessary funding, supervised the entire study and wrote the manuscript.

Conflicts of interest

There are no conflicts to declare.

Acknowledgements

The project leading to this publication has received funding from Université de Reims Champagne-Ardenne and Université de Mons (Camille Gosée PhD fellowship). The authors would like to thank the "Programme de cooperation transfrontalière Interreg France-Wallonie-Vlaanderen" for its support through the "Nanocardio" project, the PHC Brancusi program (project no. 43465WA), and Nano'Mat and PlAneT platforms (supported by the European Regional Development Fund and the Region Champagne Ardenne). The CMMI and its bioprofiling platform would like to thank the European Regional Development Fund and the Walloon Region for their financial support. S. N. V. acknowledge the support of UEFISCDI within project no. 81TE/2022 (PN-IIIP1-1_1-TE-2021-1375-trans-NANO-BIO). The authors would also like to thank Thibaut Nigra for the complementary UV visible and IR analyses performed on the ZW800-1 chromophore alone and grafted to chitosan.

References

1 A. Walter, P. Paul-Gilloteaux, B. Plochberger, L. Sefc, P. Verkade, J. G. Mannheim, P. Slezak, A. Unterhuber, M. Marchetti-Deschmann, M. Ogris, K. Bühler, D. Fixler, S. H. Geyer, W. J. Weninger, M. Glösmann, S. Handschuh and T. Wanek, Correlated Multimodal Imaging in Life Sciences: Expanding the Biomedical Horizon, *Front. Phys.*, 2020, **8**, 47, DOI: **10.3389/fphy.2020.00047**.

2 C. Wang, W. Fan, Z. Zhang, Y. Wen, L. Xiong and X. Chen, Advanced nanotechnology leading the way to multimodal imaging-guided precision surgical therapy, *Adv. Mater.*, 2019, **31**, 1904329, DOI: **10.1002/adma.201904329**.

3 L. E. Jennings and N. J. Long, Two is better than one' probes for dual modality molecular imaging, *Chem. Commun.*, 2009, 3511–3524.

4 A. Louie, Multimodality Imaging Probes: Design and Challenges, *Chem. Rev.*, 2010, **110**, 3146–3195.

5 P. Verwilst, S. Park, B. Yoon and J. S. Kim, Recent advances in Gd-chelate based bimodal optical/MRI contrast agents, *Chem. Soc. Rev.*, 2015, **44**, 1791–1806.

6 X. Han, K. Xu, O. Taratula and K. Farsad, Applications of nanoparticles in biomedical imaging, *Nanoscale*, 2019, **11**, 799–819.

7 (*a*) X. Xiao, H. Cai, Q. Huang, B. Wang, X. Wang, Q. Luo, Y. Li, H. Zhang, Q. Gong, X. Ma, Z. Gu and K. Luo, Polymeric dual-modal imaging nanoprobe with two-photon aggregation-induced emission for fluorescence imaging and gadolinium-chelation for magnetic resonance imaging, *Bioact. Mater.*, 2023, **19**, 538–549; (*b*) I. Vermeulen, E. M. Isin, P. Barton, B. Cillero-Pastor and R. M. A. Heeren, Multimodal molecular imaging in drug discovery and development, *Drug Discovery Today*, 2022, **27**, 2086–2099; (*c*) H. Li, J. Sun, H. Zhu, H. Wu, H. Zhang, Z. Gu and K. Luo, Recent advances in development of dendritic polymer-based nanomedicines for cancer diagnosis, *WIREs Nanomed. Nanobiotechnol.*, 2021, **13**, e1670; (*d*) X. Xiao, H. Cai, Q. Huang, B. Wang, X. Wang, Q. Luo, Y. Li, H. Zhang, Q. Gong, X. Ma, Z. Gu and K. Luo, Enzyme-triggered deep tumor penetration of a dual-drug nanomedicine enables an enhanced cancer combination therapy, *Bioact. Mater.*, 2023, **26**, 102–115; (*e*) C. Guo, L. Sun, H. Cai, Z. Duan, S. Zhang, Q. Gong, K. Luo and Z. Gu, Gadolinium-labeled biodegradable dendron–hyaluronic acid hybrid and its subsequent application as a safe and efficient magnetic resonance imaging contrast agent, *ACS Appl. Mater. Interfaces*, 2017, **9**, 23508–23519.

8 A. Gupta, P. Caravan, W. S. Price, C. Platas-Iglesias and M. Eric, Gale, Applications for transition-metal chemistry in contrast-enhanced magnetic resonance imaging, *Inorg. Chem.*, 2020, **59**, 6648–6678.

9 L. Helm, A. E. Merbach and E. Toth, *The Chemistry of Contrast Agents in Medical Magnetic Resonance Imaging*, John Wiley & Sons, Chichester, 2nd edn, 2013.

10 M. Port, J. M. Idée, C. Medina, C. Robic, M. Sabatou and C. Corot, Efficiency, thermodynamic and kinetic stability of marketed gadolinium chelates and their possible clinical consequences: a critical review, *BioMetals*, 2008, **21**, 469–490.

11 T. Courant, V. G. Roullin, C. Cadiou, M. Callewaert, M. C. Andry, C. Portefaix, C. Hoeffel, M. C. de Goltstein, M. Port, S. Laurent, L. Vander Elst, R. Muller, M. Molinari and F. Chuburu, Hydrogels incorporating GdDOTA: towards highly efficient dual T1/T2 MRI contrast agents, *Angew. Chem., Int. Ed.*, 2012, **51**, 9119–9122.

12 M. Callewaert, V. G. Roullin, C. Cadiou, E. Millart, L. Van Gulik, M. C. Andry, C. Portefaix, C. Hoeffel, S. Laurent, L. Vander Elst, R. Muller, M. Molinari and F. Chuburu, Tuning the composition of biocompatible Gd nanohydrogels to achieve hypersensitive dual T1/T2 MRI contrast agents, *J. Mater. Chem. B*, 2014, **2**, 6397–6405.

13 J. Moreau, M. Callewaert, V. Malytskyi, C. Henoumont, S. N. Voicu, M. S. Stan, M. Molinari, C. Cadiou, S. Laurent and F. Chuburu, Fluorescent chitosan-based nanohydrogels and encapsulation of gadolinium MRI contrast agents for magneto-optical imaging, *Carbohydr. Polym. Technol. Appl.*, 2021, **2**, 100104.

14 Z. T. Rosenkrans, C. A. Ferreira, D. Ni and W. Cai, Internally responsive nanomaterials for activatable multi-

modal imaging of cancer, *Adv. Healthcare Mater.*, 2021, **10**, 2000690.

15 M. Liu, R.-C. Anderson, X. Lan, P. S. Conti and K. Chen, Recent advances in the development of nanoparticles for multimodality imaging and therapy of cancer, *Med. Res. Rev.*, 2020, **40**, 909–930.

16 S. Zackrisson, S. M. W. Y. van de Ven and S. S. Gambhir, Light in and sound out: emerging translational strategies for photoacoustic imaging, *Cancer Res.*, 2014, **74**, 979–1004.

17 V. Ntziachristos and D. Razansky, Molecular imaging by means of multispectral optoacoustic tomography (MSOT), *Chem. Rev.*, 2010, **110**, 2783–2794.

18 A. B. Ebrahim Attia, G. Balasundaram, M. Moothanchery, U. S. Dinish, R. Bi, V. Ntziachristos and M. Olivo, A review of clinical photoacoustic imaging: Current and future trends, *Photoacoustics*, 2019, **16**, 100144.

19 I. Steinberg, D. M. Huland, O. Vermesh, H. E. Frostig, W. S. Tummers and S. S. Gambhir, Photoacoustic clinical imaging, *Photoacoustics*, 2019, **14**, 77–98.

20 H. Hyun, M. W. Bordo, K. Nasr, D. Feith, J. H. Lee, S. H. Kim, Y. Ashitate, L. A. Moffitt, M. Rosenberg, M. Henary, H. S. Choi and J. V. Frangioni, GMP-Compatible preparative scale synthesis of near-infrared fluorophores, Contrast Media Mol, *Imaging*, 2012, **7**, 516–524.

21 V. T. C. Tsang, X. Li and T. T. W. Wong, A review of endogenous and exogenous contrast agents used in photoacoustic tomography with different sensing configurations, *Sensors*, 2020, **20**, 5595, DOI: **10.3390/s20195595**.

22 V. Gujrati, A. Mishra and V. Ntziachristos, Molecular imaging probes for multi-spectral optoacoustic tomography, *Chem. Commun.*, 2017, **53**, 4653–4672.

23 J. Weber, P. C. Beard and S. E. Bohndiek, Contrast agents for molecular photoacoustic imaging, *Nat. Methods*, 2016, **16**, 639–650.

24 L. Nie and X. Chen, Structural and functional photoacoustic molecular tomography aided by emerging contrast agents, *Chem. Soc. Rev.*, 2014, **43**, 7132–7170.

25 Y. Wu, F. Zeng, Y. Zhao and S. Wu, Emerging contrast agents for multispectral optoacoustic imaging and their biomedical applications, *Chem. Soc. Rev.*, 2021, **50**, 7924–7940; Z. Zhao, C. B. Swartchick and J. Chan, Targeted contrast agents and activatable probes for photoacoustic imaging of cancer, *Chem. Soc. Rev.*, 2022, **51**, 829–868.

26 J. E. Lemaster and J. V. Jokerst, What is new in nanoparticle-based photoacoustic imaging?, *WIREs Nanomed. Nanobiotechnol.*, 2017, **9**, e1404, DOI: **10.1002/wnan.1404**.

27 Z. Sang, J. Quan, J. Han, X. Deng, J. Shen, G. Li and Y. Xie, Comparison of three water-soluble polyphosphate tripolyphosphate, phytic acid, and sodium hexametaphosphate as crosslinking agents in chitosan nanoparticle formulation, *Carbohydr. Polym.*, 2020, **230**, 115577.

28 H. S. Choi, K. Nasr, S. Alyabyev, D. Feith, J. H. Lee, S. H. Kim, Y. Ashitate, H. Hyun, G. Patonay, L. Strekowski, M. Henary and J. V. Frangioni, Synthesis and in vivo fate of zwitterionic near-infrared fluorophores, *Angew. Chem., Int. Ed.*, 2011, **50**, 6258–6263.

29 J. D. Robertson, L. Rizzello, M. Avila-Olias, J. Gaitzsch, C. Contini, M. S. Magoń, S. A. Renshaw and G. Battaglia, Purification of nanoparticles by size and shape, *Sci. Rep.*, 2016, **6**, 27494–27501.

30 T. Mosmann, Rapid colorimetric assay for cellular growth and survival: application to proliferation and cytotoxicity assays, *J. Immunol. Methods*, 1983, **65**, 55–63.

31 H. Hyun, E. A. Owens, L. Narayana, H. Wada, J. Gravier, K. Bao, J. V. Frangioni, H. S. Choi and M. Henary, Central C–C bonding increases optical and chemical stability of NIR fluorophores, *RSC Adv.*, 2014, **4**, 58762.

32 F. A. Oyarzun-Ampuero, J. Brea, M. L. Loza, D. Torres and M. J. Alonso, Chitosan–hyaluronic acid nanoparticles loaded with heparin for the treatment of asthma, *Int. J. Pharm.*, 2009, **381**, 122–129.

33 A. Z. Khawaja, D. B. Cassidy, J. Al Shakarchi, D. G. McGrogan, N. G. Inston and R. G. Jones, Revisiting the risks of MRI with gadolinium based contrast agents—review of literature and guidelines, *Insights Imaging*, 2015, **6**, 553–558.

34 E. Gianolio, P. Bardini, F. Arena, R. Stefania, E. Di Gregorio, R. Iani and S. Aime, Gadolinium retention in the rat brain: assessment of the amounts of insoluble gadolinium-containing species and intact gadolinium complexes after repeated administration of gadolinium-based contrast agents, *Radiology*, 2017, **285**, 839–849.

35 G. Rigaux, C. V. Gheran, M. Callewaert, C. Cadiou, S. N. Voicu, A. Dinischiotu, M. C. Andry, L. Vander Elst, S. Laurent, R. N. Muller, A. Berquand, M. Molinari, S. Huclier-Markai and F. Chuburu, Characterization of Gd loaded chitosan-TPP nanohydrogels by a multi-technique approach combining dynamic light scattering (DLS), asymmetrical flow-field-flow fractionation (AF4) and atomic force microscopy (AFM) and design of positive contrast agents for molecular resonance imaging (MRI), *Nanotechnology*, 2017, **28**, 055705.

36 L. Q. Jiang, T. Y. Wang, T. J. Webster, H. J. Duan, J. Y. Qiu, Z. M. Zhao and C. L. Zheng, Intracellular disposition of chitosan nanoparticles in macrophages: intracellular uptake, exocytosis, and intercellular transport, *Int. J. Nanomed.*, 2017, **12**, 6383–6388.

37 C. V. Gheran, G. Rigaux, M. Callewaert, A. Berquand, M. Molinari, F. Chuburu, S. N. Voicu and A. Dinischiotu, Biocompatibility of Gd-loaded chitosan-hyaluronic acid nanogels as contrast agents for magnetic resonance cancer imaging, *Nanomaterials*, 2018, **8**, 201.

38 F. Carniato, M. Ricci, L. Tei, F. Garello, E. Terreno, E. Ravera, G. Parigi, C. Luchinat and M. Botta, High relaxivity with no coordinated waters: a seemingly paradoxical behavior of $[Gd(DOTP)]^{5-}$ embedded in nanogels, *Inorg. Chem.*, 2022, **61**, 5380–5387.

39 F. Carniato, L. Tei, M. Botta, E. Ravera, M. Fragai, G. Parigi and C. Luchinat, ^{1}H NMR relaxometric study of chitosan-based nanogels containing mono- and bis-hydrated Gd(III)

chelates: clues for MRI probes of improved sensitivity, *ACS Appl. Bio Mater.*, 2020, **3**, 9065–9072.

40 M. Russo, A. M. Ponsiglione, E. Forte, P. A. Netti, E. Torino and E. Hydrodenticity, to enhance relaxivity of gadolinium DTPA within crosslinked hyaluronic acid nanoparticles, *Nanomedicine*, 2017, **12**, 2199–2210.

41 F. De Sarno, A. M. Ponsiglione, M. Russo, A. M. Grimaldi, E. Forte, P. A. Netti and E. Torino, Water-mediated nanostructures for enhanced MRI: impact of water dynamics on relaxometric properties of Gd-DTPA, *Theranostics*, 2019, **9**, 1809–1824.

42 A. Basu, K. R. Kunduru, E. R. Abtew and R. T. Domb, Polysaccharide-Based Conjugates for Biomedical Applications, *Bioconjugate Chem.*, 2015, **26**, 1396–1412.

43 S. Aime, D. Delli Castelli, D. Lawson and E. Terreno, Gd-loaded liposomes as T1, susceptibility, and CEST agents, all in one, *J. Am. Chem. Soc.*, 2007, **129**, 2430–2431.

44 M. Devreux, C. Henoumont, F. Dioury, D. Stanicki, S. Boutry, L. Larbanoix, C. Ferroud, R. N. Muller and S. Laurent, Bimodal Probe for Magnetic Resonance Imaging and Photoacoustic Imaging Based on a PCTA-Derived Gadolinium(III) Complex and ZW800–1, *Eur. J. Inorg. Chem.*, 2019, 3354–3365.